

X-RAY EMISSION FROM MEGAMASER GALAXY IC 2560

G. MADEJSKI,^{1,2} C. DONE,³ P. T. ŻYCKI,⁴ AND L. GREENHILL^{2,5}

Received 2005 June 3; accepted 2005 September 8

ABSTRACT

An observation of the H₂O megamaser galaxy IC 2560 with the *Chandra X-Ray Observatory* reveals a complex spectrum composed of soft X-ray emission due to multitemperature thermal plasma and a hard continuum with strong emission lines. The continuum is most likely a Compton reflection (reprocessing) of primary emission that is completely absorbed at least up to 7 keV. The lines can be identified with fluorescence from Si, S, and Fe in the lowest ionization stages. The equivalent widths of the Si and S lines are broadly compatible with those anticipated for reprocessing by optically thick cold plasma of solar abundances, while the large equivalent width of the Fe line requires some overabundance of iron. A contribution to the line from a transmitted component cannot be ruled out, but the limits on the strength of the Compton shoulder make it less likely. From the bolometric luminosity of the nuclear region, we infer that the source radiates at 1%–10% of its Eddington luminosity for an adopted central mass of $3 \times 10^6 M_{\odot}$. The overall spectrum is consistent with the hypotheses that the central engines powering the detected megamasers in accretion disks are obscured from direct view by the associated accretion disk material itself and that there is a correlation between the occurrence of megamaser emission and Compton-thick absorption columns. For the 11 known galaxies with both column density measurements and maser emission believed to arise from accretion disks, eight AGNs are Compton thick.

Subject headings: galaxies: active — galaxies: individual (IC 2560) — masers — X-rays: galaxies

Online material: color figures

1. INTRODUCTION

Position-velocity-resolved interferometric mapping of water vapor maser emission ($\nu_{\text{rest}} = 22235.08$ MHz) in active galactic nuclei (AGNs) is a powerful tool for the study of gas structures and dynamics in regions less than of order 1 pc from massive central engines. For the cases in which the megamaser emission can be identified with an accretion disk rather than with the wind- or jetlike outflow, such mapping may allow the determination of central engine (and presumably black hole) mass, Eddington luminosity, and disk geometry (e.g., warping). The three most notable examples are the geometrically thin accretion disk of NGC 4258 (Miyoshi et al. 1995; Greenhill et al. 1995), which obeys a Keplerian rotation law to $\ll 1\%$; the apparently massive accretion disk within the NGC 1068 AGN (Greenhill et al. 1997; Kumar 1999; Lodato & Bertin 2003); and the accretion disk within the nucleus of the Circinus galaxy (Greenhill et al. 2003) and the associated wide-angle wind.

Water megamaser and nuclear activities are linked by the maser pump process, which in the case of accretion disks is plausibly driven by collisions in molecular gas heated by X-ray irradiation (Neufeld et al. 1994). Nonetheless, detectable megamaser emission is relatively rare. This is probably a consequence of intrinsic luminosity and geometry. In general, maser emission is amplified most along the directions in which there is the most material with overlapping line-of-sight velocities, and as a result the emission is beamed narrowly along tangent planes for

any individual accretion disk. Association with type 2 AGNs is a consequence.

Average detection rates among type 2 AGNs are on the order of 10% (e.g., Braatz et al. 2004), depending on galaxy distance and instrument sensitivity. Only ~ 60 megamaser systems are known (Kondratko et al. 2006a; P. T. Kondratko et al. 2006b, in preparation; Henkel et al. 2005 and references therein), and evidence from spectra and Very Long Baseline Interferometer (VLBI) maps associating the emission with accretion disks is available for about a third (e.g., Kondratko et al. 2005). Nonetheless, the contribution to understanding of AGNs by broadband studies of megamaser galaxies lies in the qualitatively greater level of detail that may be achieved, specifically because the structure and dynamics of the molecular gas can be so well constrained.

Although the central engines associated with megamasers are likely to be obscured in the optical, UV, and soft X-ray bands—at least for the absorbing columns corresponding to less than a few Thomson optical depths—X-ray spectroscopy can provide a good estimate of the absorbing column and thus the true luminosity of the central source. For other, more heavily obscured sources, the details of the profile of the Fe K α line can often provide additional constraints (e.g., Levenson et al. 2002). One good candidate for detailed measurements is the Seyfert 2 galaxy IC 2560. It contains an H₂O megamaser (Braatz et al. 1996) with a peak flux density of up to ~ 0.4 Jy. This relatively nearby (26 Mpc; $v_{\text{rec}} = 2876$ km s⁻¹) source has been partially resolved with the VLBI (Ishihara et al. 2001), and a central black hole mass of $\sim 3 \times 10^6 M_{\odot}$ was inferred, which is relatively low but comparable to the mass of the black hole in our own Milky Way (Ghez et al. 2005; Schödel et al. 2003) and that in the Circinus galaxy (Greenhill et al. 2003).

Prior to the observation described in § 2, this object has been observed with *Chandra* in 2000 October, via a short (~ 10 ks) observation reported in Iwasawa et al. (2002), and even before that with the *Advanced Satellite for Cosmology and Astrophysics*

¹ Stanford Linear Accelerator Center, 2575 Sand Hill Road, Menlo Park, CA 94025; madejski@stanford.edu.

² Kavli Institute for Particle Astrophysics and Cosmology, Stanford, CA 94305.

³ Department of Physics, Durham University, Durham, UK.

⁴ Nicolaus Copernicus Astronomical Center, Warsaw, Poland.

⁵ Harvard-Smithsonian Center for Astrophysics, Cambridge, MA 02138.

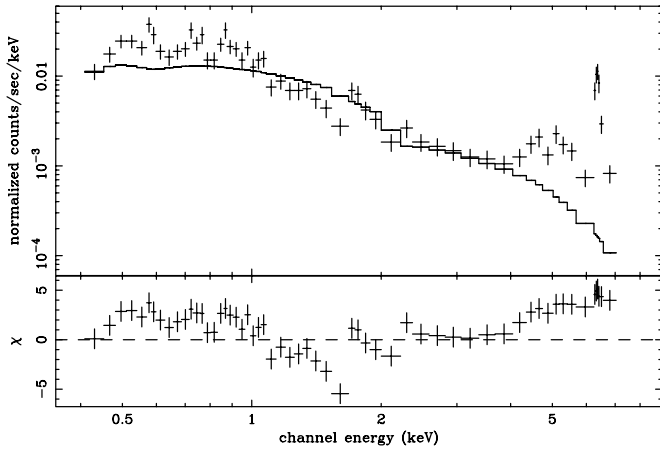


FIG. 1.—*Chandra* count spectrum for IC 2560, fitted to a simple power-law model, absorbed at low energies by the Galactic absorption of $6.5 \times 10^{20} \text{ cm}^{-2}$. The residuals to the fit (plotted as the contribution to χ^2) show strong residual features, modeled and discussed in § 2.

(Ishihara et al. 2001). The data reported here are based on a longer, 50 ks pointing obtained in 2004 February.

2. OBSERVATIONS, DATA REDUCTION, AND SPECTRAL FITTING

A 50 ks *Chandra* observation of IC 2560 was conducted on 2004 February 16–17. The processed data were reduced using the XSELECT tool, with an independent analysis using CIAO. Data were collected with the Advanced CCD Imaging Spectrometer (ACIS-S), with the source on chip S3. The intensity of un-rejected background was constant and relatively low (less than 2 counts s^{-1} in the entire ACIS-S3 chip), showing no sign of any flares, so removal of any additional data segments was not necessary. The image consists mainly of the point source, but there is a hint of some extended component. The spectrum of the extended component is under investigation. To measure the spectrum of the nuclear source, we extracted the data from a region $2''$ (~ 250 pc) in radius and determined the background from an annulus with inner radius $30''$ and outer radius $90''$ centered on the source. These correspond to roughly 3.8 and 11.3 kpc at the source’s distance, and while this might also include some of the diffuse emission from the galaxy itself, in the quite compact source region chosen here the contribution of such diffuse emission (or

instrumental background) was negligible, less than 0.1% of the source count rate. The total net count rate in the 0.5–10.0 keV range was 0.025 counts s^{-1} . The spectrum was subsequently rebinned to allow at least 20 counts in a new spectral bin. We note that there is no variability in the source flux during the *Chandra* observation. Furthermore, the source shows the same count rate—as well as flux, for the same assumed models—as reported in Iwasawa et al. (2002). We prepared the ACIS-S3 redistribution matrices and the effective area files as appropriate for this observation. Since the data were taken relatively recently, the charge transfer inefficiency (CTI) correction has been applied in the course of the pipeline processing.

The background-subtracted data are well represented by a spectrum with three general components: a very hard continuum, a soft component with some soft X-ray emission lines, and an emission-line complex between 6 and 7 keV, presumably due to Fe K-shell transitions. This is illustrated in Figure 1, where we assumed as a model a simple power law absorbed by the Galactic column of $6.5 \times 10^{20} \text{ cm}^{-2}$. The residuals clearly show the features above. This spectrum is similar to that reported by Iwasawa et al. (2002), but the longer exposure clearly reveals more details, with better resolved spectral features. A somewhat more complex and realistic model including a power law, collisionally ionized plasma (described as a MEKAL XSPEC model; see below), and Gaussian line, respectively, for the hard continuum, soft emission, and the Fe line gives an energy power-law index $\alpha = -1.3 \pm 0.3$ (Table 1, model 1). This is extremely hard for the intrinsic X-ray spectrum of an AGN, but since IC 2560 is a megamaser source, the AGN might be obscured by a large column of absorbing material, and the continuum measured here is probably not the primary spectrum. Specifically, the primary continuum might well be a power law, but we anticipate that it is heavily absorbed rather than particularly hard (as compared to unobscured Seyfert galaxies), and it may be accompanied by a Compton reflection component, which is likely to be present when the primary source photons are reprocessed by circumnuclear material. If the absorption is particularly severe, $\sim 10^{25} \text{ cm}^{-2}$ or more for solar abundances, then the very hard spectrum measured above ~ 2.5 keV could be just that due to the reflected component, although some additional flux might arise via transmission through the absorber.

Below, we describe the hard continuum as pure Compton reflection. When we replace the power-law component representing the primary continuum with a reflection component at a fixed 60° inclination (using the XSPEC model `pexrav`; see Magdziarz

TABLE 1
RESULTS OF DATA MODELING WITHOUT PHOTOIONIZATION

Model ^a	kT_1^b (keV)	A_1^b	kT_2^b (keV)	A_2^b	Γ^c	EW ^d (keV)	χ^2/dof
1 mk+po+ga.....	$0.53^{+0.13}_{-0.09}$	$0.019^{+0.014}_{-0.013}$	-0.3 ± 0.3	2.7 ± 0.5	89.6/49
2 mk+rf+ga.....	$0.58^{+0.10}_{-0.14}$	$0.023^{+0.023}_{-0.14}$	$2.24^{+0.45}_{-0.39}$	$2.8^{+0.07}_{-0.6}$	90.2/49
3 2mk+rf+ga.....	$0.65^{+0.10}_{-0.06}$	1 ^e	$0.14^{+0.05g}_{-0.05}$	1 ^e	2.8 ± 0.2	$3.6^{+0.8}_{-0.6}$	83.7/48
4 2mk+rf+3ga ^f	$0.65^{+0.10}_{-0.06}$	1 ^e	$0.14^{+0.04g}_{-0.06}$	1 ^e	$2.7^{+0.2}_{-0.3}$	3.4 ± 0.7	71.1/44
5 ab+2mk+rf+3ga+ds ^h	$0.58^{+0.07}_{-0.13}$	1 ^e	$0.08^{+0.02g}_{-0}$	1 ^e	2.2 ± 0.5	$2.7^{+0.4}_{-0.6}$	61/42

^a Model names describe spectral forms incorporated into the model: mk, MEKAL; po, power law; ga, Gaussian line; rf, Compton reflection (`pexrav`); 3ga, three Gaussian lines; ds, Compton downscattered line shoulder; and ab, additional absorption at redshift $z = 0.01$ of host galaxy.

^b MEKAL model plasma temperature and metal abundances.

^c Power-law photon spectral index, $N(E) \propto E^{-\Gamma}$.

^d EW is the equivalent width of the Fe 6.4 keV line.

^e Parameter fixed; the abundances are not well constrained ($0.2 < A < 1$).

^f Three Gaussian lines are the Fe K, Si K, and S K lines originating in neutral material, as described in the text.

^g Parameter uncertainty pegged at lower limit.

^h Host galaxy $N_{\text{H}} = 0.66^{+0.08}_{-0.24} \times 10^{22} \text{ cm}^{-2}$, and upper limit to the downscattered/observed line intensity is ~ 0.15 .

& Zdziarski 1995), we obtain $\alpha = 1.3_{-0.4}^{+0.3}$, which corresponds to a more reasonable intrinsic spectrum of the illuminating photons. The choice of a pure reflection model is also supported by the detection of the very strong, intrinsically narrow Fe K line (equivalent width ~ 2.5 keV, depending on the adopted continuum model, and $\sigma < 40$ eV) at an energy of $6.40_{-0.2}^{+0.1}$ keV, which is consistent with neutral material and in agreement with Iwasawa et al. (2002). The soft component below 1 keV is fairly well fit by a single-temperature, collisionally ionized plasma with $kT = 0.5 \pm 0.1$ keV, but with unphysically low abundances $A = 0.02 \pm 0.01$ (Table 1, model 2).

The strong iron line should also be accompanied by a noticeable Compton downscattered shoulder, forming a continuum centered at a rest-frame energy of ~ 6.3 keV with an intrinsic width of ~ 0.14 keV (Illarionov et al. 1979). The strength of this continuum relative to the unscattered narrow-line core depends on the details of the reflecting material (Matt 2002; see Fig. 2). This component has been seen in other reflection-dominated AGNs, such as the Circinus galaxy (Molendi et al. 2003), NGC 4945 (Done et al. 2003), and NGC 1068 (Matt et al. 2004). We incorporated the shape of this downscattered continuum (Illarionov et al. 1979) as a local model in XSPEC, assuming a temperature of 1 eV for the reflecting material, and include it in the spectral fit in Table 1, model 5. While this downscattered continuum is not significantly detected in our data, the 90% confidence upper limit on its strength is $\sim 15\%$ of that of the narrow-line core. The low value indicates supersolar iron abundance, with the observed flux arising from a reflector viewed at a high inclination (Matt 2002), as may be anticipated for reflection from the far side of a flattened structure with a fairly constant ratio of height to radius.

In addition to the 6.4 keV line, there is probably a marginally resolved line at 6.7 keV as well, although it is not highly significant (and thus not included in any fits in Table 1): adding three parameters improves the best-fit χ^2 only by 5. Close inspection of the unbinned data does not reveal whether the line is intrinsically broad or divisible into subcomponents, but the latter is a more likely possibility. If real, the 6.7 keV emission indicates very hot or highly ionized material, in contrast to the neutral material responsible for the 1.75 (Si) and 2.32 keV (S) lines discussed below and the Compton reflecting material, which has a lower inferred ionization parameter. The presence of 6.7 keV emission provides marginal evidence of a multitemperature plasma in close proximity to the central engine.

Rather than a very low abundance single-temperature plasma, the soft spectrum may be well fit by a model comprising nearly solar abundance material, but also including a second plasma component with $kT \sim 0.1$ keV. The new component contributes the additional continuum necessary to dilute model line strengths and match the observations with more typical abundances (Table 1 as model 3). These two temperature components are probably simply an approximation to the multitemperature hot gas that is expected in starburst regions (e.g., Strickland & Stevens 2000). It should not be confused with the multitemperature plasma inferred from the Fe line emission, which originates on much smaller scales. We note here that even though a two-temperature model is consistent with solar abundances, it constrains them poorly: spectral fits—where we require the same abundance of both MEKAL components—allow abundances ranging from 0.2 to 1. We note here that it is possible to fit the spectrum with a combination of thermal plasma and photoionized components, but at least some contribution from thermal plasma is required; we discuss this more extensively below. However, there is *no* combination of hot gas components that can account for the

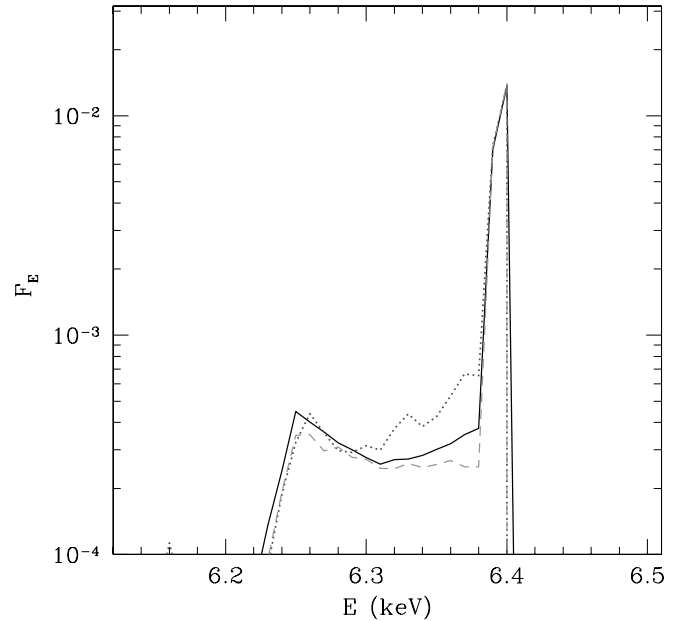


FIG. 2.—Profiles of the Fe K α line in different geometries, showing differences in the strength of the Compton shoulder. The solid curve shows the profile from transmission through a vertically extended structure (assumed to have a geometry of a torus), seen close to equatorial plane, dominated by reflection from its opposite side. The dotted curve is the profile for pure transmission through the “torus” in the equatorial plane (opposite side obscured). The dashed curve is the profile for usual Compton reflection seen at 30° . Profiles have been normalized to equal fluxes in the line core. [See the electronic edition of the Journal for a color version of this figure.]

major residuals in the spectral fit at ~ 1.8 and 2.3 keV. This is because these features are at the energies expected from *neutral* Si and S, and so cannot be produced by hot plasma emission. The obvious cool plasma component is the one that produces the reflected continuum. For solar abundances this should produce an equivalent width of ~ 250 and 170 eV in neutral Si and S, respectively (Matt et al. 1997a), to accompany the Fe line of equivalent width 0.8 – 1.6 keV (depending on atomic data and assumed geometry: George & Fabian 1991; Życki & Czerny 1994; Matt et al. 1996). Adding in two additional Gaussian lines gives line emission with an equivalent width of 130_{-80}^{+90} eV at 1.75 ± 0.03 keV for Si and of 200 ± 140 eV at 2.32 ± 0.12 keV for S, accompanying the neutral fluorescent iron line of large equivalent width, 3.4 ± 0.7 keV (Table 1, model 4). Thus, while the Si and S line energies and strengths are consistent (although with fairly large error bars) with the fluorescent lines expected from reflection from X-ray-illuminated neutral material with solar abundances, the iron line is relatively strong, which indicates supersolar abundances in this element.

There is some evidence for additional cold photoelectric absorption, with the best fit yielding $N_{\text{H}} \sim (50\text{--}70) \times 10^{20} \text{ cm}^{-2}$ in addition to the $6.5 \times 10^{20} \text{ cm}^{-2}$ attributable to our Galaxy. This inference depends on the description of the hot gas component: this is because the abundances and relative intensities in the MEKAL plasma are strongly correlated with the inferred level of photoelectric absorption in the spectral fitting. In any case, such columns are generally seen toward starbursts, as expected from the molecular gas in these regions (e.g., Pietsch et al. 2001). Note that this is in contrast to the *primary* continuum of the AGN, which we assume to have *very large* absorption, $> 10^{24} \text{ cm}^{-2}$. The model including such additional absorption is given in Table 1 as model 5.

Although the observed soft X-ray emission is consistent with arising in a gas-rich, dusty starburst region, there is a potential

TABLE 2
RESULTS OF DATA MODELING WITH PHOTOIONIZATION MODELS

Model ^a	$\log(\xi_1)^b$	$\log(\xi_2)^b$	kT^c (keV)	Γ^d	EW ^e (keV)	χ^2/dof
1 xstar ^f +rf+3ga.....	1.6	$3.11^{+0.14}_{-0.15}$	$4.6^{+1.0}_{-0.8}$	152/49
2 xstar ^f +po+rf+3ga.....	1.6	$2.2^{+0.3}_{-0.4}$	3.5	106/48
3 xstar ^f +mk+rf+3ga.....	3.0	...	$0.23^{+0.03}_{-0.01}$	$1.5^{+0.5}_{-0.4}$	$2.7^{+0.3}_{-0.8}$	89.4/47
4 2xstar ^f +rf+3ga.....	3.0	1.4	...	$1.5^{+0.5}_{-0.4}$	2.4 ± 0.5	96.4/47
5 2xstar ^f +mk+rf+3ga.....	3.0	1.6 ± 0.2	0.19 ± 0.03	1.6 ± 0.4	2.40 ± 0.45	58.1/45

^a Spectral components: xstar, XSTAR photoionization model; mk, MEKAL; po, power law; rf, Compton reflection (pexrav); and 3ga, three Gaussian lines.

^b Log of ionization parameter in XSTAR model.

^c Plasma temperature in MEKAL model.

^d Power-law photon spectral index, $N(E) \propto E^{-\Gamma}$.

^e EW is the equivalent width of the Fe 6.4 keV line.

^f Model parameterized by ionization parameter ξ and H column density N_H . Fits show no dependence on N_H , and uncertainties on $\log(\xi)$ are usually smaller than the model grid spacing [$\Delta \log(\xi) = 0.2$] and are not shown.

alternative origin via *scattering* in partially ionized material. Such extended emission from photoionized gas is seen in the soft X-ray spectra of other AGNs (e.g., Mrk 3; Sako et al. 2000). Here we investigate the origin of this emission by replacing the two MEKAL plasma components with the emission expected from photoionized gas (modeled using the XSTAR code; Bautista & Kallman 2001; grid19c from the XSTAR Web page). A simple model with one XSTAR component replacing the two MEKAL components (from model 4 in Table 1) gives a bad description of data, $\chi^2_\nu = 152/49$ (model 1 in Table 2). The fit can be improved by adding a power law representing the primary emission scattered off a completely ionized plasma, but the fit is still unsatisfactory ($\chi^2_\nu = 106/48$; model 2 in Table 2), with strong residuals around 0.6 and 1 keV. However, previous fits indicate that the emitting plasma is multitemperature; therefore, we also try more complex models. Two photoionized XSTAR components (with different ionization parameters) give a better fit, $\chi^2_\nu = 96.4/47$ (model 4), but strong residuals still remain at low energies. These residuals cannot be explained by any pair of photoionized components, but inclusion of an additional MEKAL component provides a satisfactory fit, giving $\chi^2_\nu = 58.1/45$ (model 5). For completeness, we have also investigated a simpler hybrid model with one XSTAR and one MEKAL component (model 3), but this gives an unsatisfactory fit, $\chi^2_\nu = 89.4/47$. Thus, at least some contribution from mechanically heated plasma is necessary to explain the soft X-ray emission, but even then the photoionized plasma has to have a range of ionization stages. The presence of mechanically (collisionally) heated plasma is in fact expected in IC 2560, as the galaxy contains a starburst region (Cid Fernandes et al. 2004).

To quantify this, we investigated the relative fluxes of the MEKAL and photoionized plasmas. The two MEKAL components in model 5 of Table 1 contribute comparably, at the observed flux level of $\sim 2 \times 10^{-14}$ ergs cm⁻² s⁻¹. In the hybrid model, model 5 of Table 2, the MEKAL component contributes comparably to that in low- T component in the two-MEKAL model ($\sim 2 \times 10^{-14}$ ergs cm⁻² s⁻¹), while the sum of the two XSTAR components contributes $\sim 5 \times 10^{-14}$ ergs cm⁻² s⁻¹. This leads us to the conclusion that the total contribution of photoionized emission to the soft X-ray flux of IC 2560 can be as little as 0% and much as $\sim 70\%$ of the total, but (1) at least some collisionally heated plasma is required, and (2) the photoionized component implies a wide range of ionization parameters.

Hence, we use the best-fit starburst/reflection-dominated AGN model (that given in Table 1 as model 5) to plot the unfolded

spectrum shown in Figure 3. A remaining small residual can be seen at ~ 5 keV. Including a free Gaussian line to model this feature gives a better fit with $\chi^2_\nu = 46.9/39$, formally a significant detection with a line energy of 5.1 ± 0.2 keV, a width of $0.5^{+0.3}_{-0.4}$ keV, and a very large equivalent width of $1.5^{+2.0}_{-1.2}$ keV. However, no plausible atomic features exist at this energy. At such a high equivalent width it is most likely to be iron, but the energy shift is very large, requiring the material to be flowing away from the observer at $\sim 50,000$ km s⁻¹. A multiple Compton downscattered shoulder explanation seems even more contrived. However, this best fit also requires that the reflected emission is now due to an unusually steep power law illuminating the reflector, with an energy spectral index of $\alpha = 2.1$. Assuming that

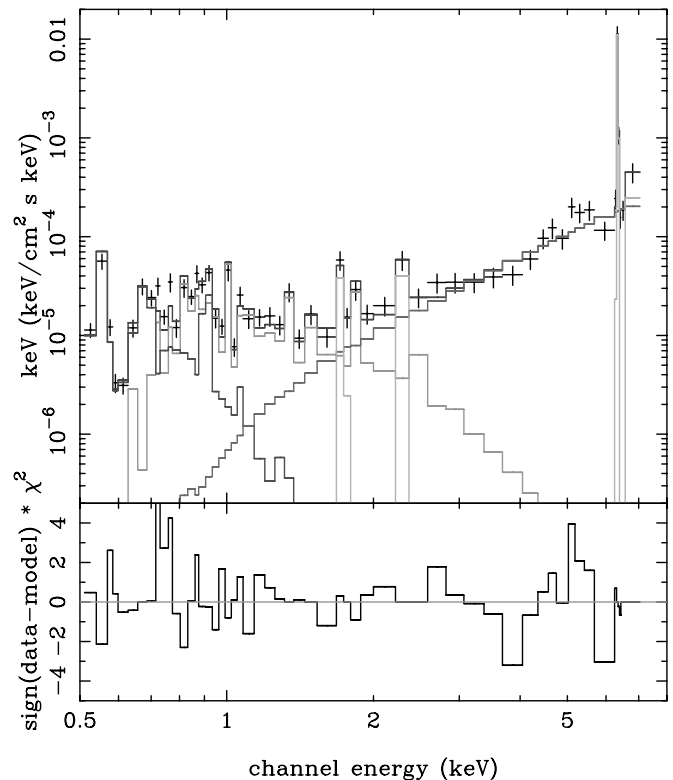


FIG. 3.—Unfolded spectrum of IC 2560, as collected by *Chandra* in 2004. The model spectrum includes the Compton reflection of the invisible continuum, the two thermal plasma components, and the emission lines, as discussed in the text. [See the electronic edition of the *Journal* for a color version of this figure.]

the intrinsic AGN spectrum has a more usual $\alpha = 1$ gives $\chi^2_\nu = 54.3/40$, compared to 57.7/43 without the additional line, so it is not significant on an F -test. Thus, it seems most likely that this feature may be an artifact in a complex, low signal-to-noise ratio spectrum.

With such a model, and including the emission lines as given below, the measured total 2–10 keV flux is 3.3×10^{-13} ergs cm $^{-2}$ s $^{-1}$. When the emission lines discussed below are accounted for separately, then the measured reflection model flux (and this of course does not include the primary continuum) is 2.6×10^{-13} ergs cm $^{-2}$ s $^{-1}$. In the extreme case, if the reflector were to subtend a solid angle as large as 2π , it would have to be illuminated by an intrinsic, unabsorbed (but invisible directly to the observer) 2–10 keV flux of 4.5×10^{-12} ergs cm $^{-2}$ s $^{-1}$. A more likely geometry might be one in which a much smaller fraction of the reflector is visible to us, in which case the unabsorbed flux of the AGN is correspondingly higher. We can thus set a lower limit on the 2–10 keV luminosity of $\sim 3 \times 10^{41}$ ergs s $^{-1}$; at least this much is needed to account for the reflected spectrum.

3. ORIGIN OF THE X-RAY SPECTRAL FEATURES AND THE RELATIONSHIP OF THE MEGAMASER EMISSION TO THE X-RAY ABSORPTION

The spectral fits presented in § 2 indicate that the iron $K\alpha$ line is somewhat stronger than predicted, perhaps indicating a supersolar iron abundance. We quantify this by a Monte Carlo simulation of reflection from a square cross section torus-like structure with Thomson optical depth $\tau_T = 3$, with an inner edge starting 50° from the “torus” axis (see Krolik et al. 1994). This gives a predicted iron $K\alpha$ line equivalent width of 1.5 keV (Anders-Grevesse abundances: Fe/H = 4.7×10^{-5}) or 1.2 keV (Anders-Ebihara abundances: Fe/H = 3.3×10^{-5}) for viewing angles close to the equatorial plane. To get a reflected iron line as large as that observed requires at least 2 times the solar abundance of Fe. The large iron $K\alpha$ line also should be accompanied by strong $K\beta$ emission at 7.05 keV, whose strength is about 10% of that of the $K\alpha$ line. While the signal-to-noise ratio at these high energies is not high, such a feature (with all parameters fixed or tied to $K\alpha$) reduces χ^2_ν by 3 to 57.8/42.

An alternative explanation for a large iron line equivalent width is the contribution from a heavily absorbed *transmitted* spectrum as well as reflection (Ghisellini et al. 1994; Levenson et al. 2002). If the observed line is indeed due to transmission, it would imply that the direct component, expected at 20–100 keV, should be quite strong, as in the case of NGC 4945 (Done et al. 1996). However, with solar abundances this would require the model torus to subtend a rather large solid angle with a polar opening angle of $\leq \pm 15^\circ$ (Levenson et al. 2002). The Compton downscattered shoulder would also be stronger than that seen in reflected emission, up to 40% of the strength of the narrow-line core (Matt 2002; see also Fig. 2), which is inconsistent with the 15% limit on the downscattered continuum estimated here.

From the spectral fits described in Tables 1 and 2, a picture emerges in which the heavily absorbed primary continuum is reprocessed by nearly neutral material producing a Compton reflection component as well as fluorescence lines from Fe, S, and Si. IC 2560 joins the rather small number of AGNs (Mrk 3, Sako et al. 2000; NGC 6552, Reynolds et al. 1994) in which the fluorescence lines of species with low atomic numbers (Si and S) are seen, and thus reflected continuum in the 1–10 keV band dominates. The reflector is likely to be formed by the same optically thick material that obscures a direct view of the central engine. In IC 2560, H $_2$ O megamaser emission is also believed to arise from a close to edge-on structure (Ishihara et al. 2001),

which by analogy to the well-studied case of NGC 4258 is probably a parsec or subparsec radius annulus in an accretion disk. Geometrically, the simplest explanation of the reflector, absorber, and maser is that all three correspond to the same structure, the accretion disk. (See Greenhill et al. [2003] for discussion of similar circumstances in the Circinus galaxy.) We expect to see in reflection only a small “sliver” of this X-ray-illuminated material on the far side of the disk (a feature readily accommodated if the disk is warped), as has been observed in the megamaser galaxies NGC 4258 (Miyoshi et al. 1995) and the Circinus galaxy (Greenhill et al. 2003). Alternatively, reflection could originate from a low covering fraction, dense clouds above and below the obscuring maser structure that block our view of the central engine. The former explanation has the advantage of being simpler: only one high-column structure is required, while the latter requires different regions of optically thick material.

Regardless of the detailed location and geometry of the Compton reflector, the covering fraction of reflecting material is less than unity. This provides a lower limit to the intrinsic X-ray flux, $\sim 4 \times 10^{-12}$ ergs cm $^{-2}$ s $^{-1}$ in the 2–10 keV band, corresponding to a *minimum* bolometric (0.01–100 keV) flux of 6×10^{-11} ergs cm $^{-2}$ s $^{-1}$ and luminosity $L = 5 \times 10^{42}$ ergs s $^{-1}$. Adopting the central engine mass estimated by Ishihara et al. (2001), we can calculate $L/L_{\text{Edd}} > 0.01$. If we assume that all of the observed IR emission ($L = 3 \times 10^{43}$ ergs s $^{-1}$) is reprocessed nuclear flux, then a very conservative upper limit is $L/L_{\text{Edd}} < 0.1$. In reality, this upper limit could be reduced to account for the IR flux that might arise in the circumnuclear starburst region. With these constraints, we can infer that the accretion rate is more like that inferred for the common, broad-line Seyfert 1 galaxies (e.g., Czerny et al. 2004) and the heavily obscured (Seyfert 2) megamaser galaxies NGC 3079 (Kondratko et al. 2006a), NGC 4945 (Greenhill et al. 1997), and NGC 1068 (Greenhill & Gwinn 1997) than it is to that for the low L/L_{Edd} core of the classic megamaser galaxy NGC 4258 (e.g., Lasota et al. 1996).

IC 2560 bears a startling resemblance to NGC 4945 (Done et al. 2003; Schurch et al. 2002) in showing a reflection-dominated hard X-ray spectrum, together with starburst-dominated soft X-ray emission. In IC 2560, there is evidence for a young (≤ 25 Myr) stellar population (Cid Fernandes et al. 2004), so it seems likely that there is hot gas from a starburst providing the majority of the soft X-ray flux, rather than photoionization. These characteristics differ from those of Mrk 3 (Sako et al. 2000) and NGC 1068 (Ogle et al. 2003), which have clear signatures of predominantly photoionized soft X-ray emission. In both cases, detection of polarized broad optical emission lines indicates that there is a “mirror” directly reflecting UV and soft X-rays from the central source. Neither IC 2560 nor NGC 4945 shows broad polarized emission lines. It is worth noting here that both IC 2560 and NGC 4945 are powered by relatively low mass black holes and have modest nuclear luminosities. Low intensity in the photoionized component might be simply due to low luminosity of the central source.

A plausible scenario for many megamaser galaxies (as well as other Seyfert 2 galaxies) is that we view the primary power-law continuum of $\alpha \sim 1$ through an absorber of appreciable optical thickness. This can provide an absorbing column due to the neutral gas that might be relatively small (10^{23} cm $^{-2}$), where the primary continuum shows a modest photoelectric absorption cutoff as in Mrk 3 or NGC 4258. Alternatively, the absorber can provide a column of several times 10^{24} cm $^{-2}$ or more, as seen in NGC 4945, NGC 1068, and NGC 3079—and IC 2560 belongs to the latter group (see Table 3). For material that is optically thick to electron scattering, the primary continuum is depressed

TABLE 3
DISK MASERS IN AGNs WITH ESTIMATED COLUMN DENSITIES

GALAXY	ID ^a		N_{H} (10^{23} cm^{-2})	REFERENCES	
	VLBI	Spectra		N_{H}	Maser
NGC 4945 ^b	✓	...	45 ± 4	1	12
Circinus galaxy ^c	✓	✓	43_{-7}^{+4}	2	13
M51 ^d	✓	58_{-18}^{+38}	3	14
NGC 1386 ^e	✓	✓	>22	4	15, 16
NGC 1068.....	✓	✓	≥ 100	5	17
NGC 3079.....	✓	✓	≥ 100	6	18
IC 2560.....	...	✓	≥ 30	7, 8	19
NGC 3393.....	...	✓	44_{-11}^{+25}	4	20
NGC 4258.....	✓	✓	0.6–1.3	9	21, 22
NGC 4388 ^f	✓	0.02–4.8	10	23
NGC 4051 ^g	✓	0 (cold); 0.8–3.7 (ionized)	11	16

NOTES.—Henkel et al. (2005) and Kondratko et al. (2006a; P. T. Kondratko et al. 2006b, in preparation) list known H₂O masers in AGNs. Disk masers are those originating within accretion disks, at parsec or subparsec radii.

^a Nature of evidence supporting disk maser identification. VLBI mapping provides direct evidence. Spectra exhibiting red- and blueshifted emission (more or less) symmetrically bracketing V_{sys} provide indirect evidence. For inclusion here, offsets from systemic velocity must be $>\pm 100 \text{ km s}^{-1}$.

^b Disklike structure detected, similar to NGC 3079.

^c Column $>10^{25} \text{ cm}^{-2}$ is admitted in an alternate model.

^d Red- and blueshifted maser emission are intermittent separately.

^e VLBI detection of red side of the disk. Later detection of the blue side in spectra.

^f Classified as a Seyfert 2 galaxy, but recently exhibited large, rapid change in N_{H} .

^g Narrow-line Seyfert 1 galaxy, no neutral absorber, and ionized absorber with significant variability. Spectrum comprises narrow lines distributed over $\sim 280 \text{ km s}^{-1}$, although not well centered on V_{sys} . Hagiwara et al. (2003) infer association with an accretion disk. However, broadly spread narrow lines are also consistent with emission from a wind, as in Circinus (Greenhill et al. 2003).

REFERENCES.—(1) Madejski et al. 2000; (2) Matt et al. 1999; (3) Fukazawa et al. 2001; (4) Guainazzi et al. 2005; (5) Matt et al. 1997b; (6) Iyomoto et al. 2001; (7) Iwasawa et al. 2002; (8) this paper; (9) Fruscione et al. 2005; (10) Elvis et al. 2004; (11) McHardy et al. 1995; (12) Greenhill et al. 1997; (13) Greenhill et al. 2003; (14) Hagiwara et al. 2001; (15) Braatz et al. 1997a; (16) Hagiwara et al. 2003; (17) Greenhill & Gwinn 1997; (18) Kondratko et al. 2006a; (19) Ishihara et al. 2001; (20) P. T. Kondratko et al. 2006b, in preparation; (21) Miyoshi et al. 1995; (22) Greenhill et al. 1995; (23) Braatz et al. 2004.

at all energies. For a column with a Thomson optical depth of order unity [$N_{\text{H}} = (3\text{--}10) \times 10^{24} \text{ cm}^{-2}$], the attenuated primary spectrum can be seen above 10 keV (as in NGC 4945), but for higher columns it is completely suppressed (as in NGC 1068). The column in IC 2560 can only be constrained by the current *Chandra* data to be greater than or equal to that seen in NGC 4945, $N_{\text{H}} > 3 \times 10^{24} \text{ cm}^{-2}$. Sensitive observations at higher X-ray energies are required in order to determine whether the primary emission can be detected above 10 keV or whether like NGC 1068, IC 2560 is completely obscured along the line of sight.

The possibility of a physical association between megamaser emission and obscuring material raises the question of whether there may be a correlation between the occurrence of visible megamaser emission and detection of large obscuring columns, as hypothesized by Braatz et al. (1997b), based on a sample of five galaxies. Most importantly, maser emission is anisotropic, and for a thin, moderately warped disk it would be beamed in a narrow solid angle about the tangent planes (contingent on favorably small gradients in line-of-sight velocity). In addition, it is conceivable that maser amplification could be enhanced (i.e., longer gain paths or narrower beam angle) when large columns are present. Direct evidence that megamaser emission originates from disk material is available for about a third of the ~ 60 known masers, chiefly in the form of VLBI maps or spectra that display highly Doppler shifted line complexes symmetrically bracketing the systemic velocity (V_{sys}). Of these, there are estimates of X-ray absorption columns for 11 galaxies. Most of these systems are Compton thick; eight exhibit absorption in excess of 10^{24} cm^{-2} (Table 3). The early statistics of Braatz et al.

(1997b) (3/5) are consistent with those here (8/11), although the early subsample was not selected explicitly for “disk maser,” and reliance on *ASCA* data for estimation of columns in heavily obscured sources admitted some uncertainty. Overall, the distribution of column densities is substantially skewed with respect to the absorption distribution for type 2 AGNs in general (Bassani et al. 1999; Risaliti et al. 1999). However, three known Compton thin cases are notable: NGC 4258, NGC 4388, and NGC 4051. Each exhibits variation in column density (Fruscione et al. 2005; Elvis et al. 2004; McHardy et al. 1995). In the case of NGC 4258, the accretion disk has been shown to cross the line of sight to the central source, and modest variability in N_{H} over months is believed to arise from clumpiness at radii comparable to that of the persistent maser emission, on the order of $10^4\text{--}10^5$ Schwarzschild radii (Fruscione et al. 2005; Herrnstein et al. 2005). In contrast, NGC 4388 has displayed extreme variability in column density, on timescales as short as hours, and to values as low as $2 \times 10^{21} \text{ cm}^{-2}$. The inferred radius of the absorber is $\leq 100 R_{\text{Sch}}$ (Elvis et al. 2004). The angular structure and persistence of the maser emission is not known, but comparison to that of the absorber would enable testing of whether both arise from the same (disklike) structure. The third AGN, NGC 4051, is unusual in that it is a narrow-line Seyfert 1 galaxy yet hosts a maser source that has been suggested to arise in a central accretion disk (Hagiwara et al. 2003). Column density variation is evident (McHardy et al. 1995), but unlike NGC 4258 and NGC 4388, the absorber is ionized and unlikely to lie physically close to the maser medium. It is unlikely that there is any edge-on structure comprising cold material that could

support maser emission, and the characteristics of the maser spectrum are consistent with origin in a wind rather than a disk (see Table 3 note). This is notable given the importance of nuclear winds in the formation of narrow-line Seyfert 1 spectra. On the other hand, the absorber and maser could both trace different parts of a warped structure that is only moderately inclined at small radii and tangent to some lines of sight at large radii. A clumpy or frothy medium might also enable a line of sight to the central source and ionized absorber at the same time as long gain paths are achieved among clumps at larger radii.

4. SUMMARY AND CONCLUSIONS

Chandra observation of the H₂O megamaser galaxy IC 2560 reveals a complex X-ray spectrum. At low energies, it exhibits a soft spectral component that is unlikely to be characterized by a single-temperature, collisionally ionized plasma, as this would require anomalously low elemental abundances. Instead, the soft component probably arises from such plasma—presumably associated with the host galaxy—at a range of temperatures $0.1 \text{ keV} < kT < 0.7 \text{ keV}$, with abundances close to solar values. It is also possible to fit the spectrum by a model that combines one collisionally ionized plasma component and a complex photoionized scattering medium, with a range of ionization parameters.

At higher energies, the spectrum is dominated by a very hard X-ray continuum, together with several emission-line features at energies consistent with neutral Fe, Si, and S K α lines. The best interpretation of such a hard spectrum is that the primary continuum is entirely absorbed (at least in the *Chandra* bandpass), requiring $N_{\text{H}} > 0.3 \times 10^{25} \text{ cm}^{-2}$, and that we observe only the much harder Compton reflection of the hidden primary continuum from optically thick, high column density material. Given that the H₂O megamaser emission is believed to arise in a close to edge-on disklike structure and that maser action requires a large column of material, the simplest interpretation is that all three high-column, low-ionization structures (absorber, reflector, and megamaser) arise from a single physical component, probably a parsec-scale or smaller accretion disk. We hypothesize that this is the case more generally and anticipate a correlation of mega-

maser emission and high X-ray obscuration. In an initial sample of 11 galaxies, this hypothesis is borne out. Discovery of new maser sources, identification of emission origins for known sources, and measurement of X-ray spectra for host AGNs will enable further testing.

The Compton reflection from this material also produces strong fluorescent emission lines. The observed intensities of the Si and S lines are entirely consistent with reprocessing by solar abundance material, while the Fe K line, with an equivalent width of $\sim 2.5 \text{ keV}$, is a factor of 2 higher than expected. The line might arise in reflection, transmission, or both. However, the most likely explanation for the high equivalent width of the line is Compton reflection from neutral medium with supersolar (~ 2 times) Fe abundances. This is further supported by the estimated upper limit on the intensity of the Compton “shoulder” that should be associated with the Fe K line.

The intensity of the reprocessed component provides a lower limit on the 2–10 keV flux of the unabsorbed primary continuum of $4 \times 10^{-12} \text{ ergs cm}^{-2} \text{ s}^{-1}$, corresponding to a lower limit on the 0.01–100 keV luminosity of $\sim 5 \times 10^{42} \text{ ergs s}^{-1}$. Conversely, the observed bolometric luminosity of $\sim 3 \times 10^{43} \text{ ergs s}^{-1}$ places an upper limit. Since the mass of the central source estimated from partial resolution of the megamaser angular structure is $\sim 3 \times 10^6 M_{\odot}$, we infer that the source is accreting at a moderate rate corresponding to $0.01 < L/L_{\text{Edd}} < 0.1$, as is the case for other heavily absorbed megamaser galaxies (e.g., NGC 1068). Further clues to the structure of this source are likely to be revealed by sensitive hard X-ray observations at 10–50 keV, with missions such as NASA’s *Nuclear Spectroscopic Telescope Array* (*NuSTAR*).

This project was partially supported by *Chandra* grants GO4-5125X and GO4-5127X from NASA via Smithsonian Astrophysical Observatory, by the Polish KBN grants 2P03D01225 and PBZ-KBN-054/P03/2001, and by the Department of Energy contract to SLAC DE-AC3-76SF00515. L. G. thanks SLAC as well as KIPAC (Stanford University) for hospitality at the time when this research was conducted.

REFERENCES

- Bassani, L., Dadina, M., Maiolino, R., Salvati, M., Risaliti, G., della Ceca, R., Matt, G., & Zamorani, G. 1999, *ApJS*, 121, 473
 Bautista, M. A., & Kallman, T. 2001, *ApJS*, 134, 139
 Braatz, J., Greenhill, L., Moran, J., Wilson, A., & Herrnstein, J. 1997a, *BAAS*, 29, 1374
 Braatz, J. A., Henkel, C., Greenhill, L. J., Moran, J. M., & Wilson, A. S. 2004, *ApJ*, 617, L29
 Braatz, J. A., Wilson, A. S., & Henkel, C. 1996, *ApJS*, 106, 51
 ———. 1997b, *ApJS*, 110, 321
 Cid Fernandes, R., Gu, Q., Melnick, J., Terlevich, E., Terlevich, R., Kunth, D., Rodrigues Lacerda, R., & Joguet, B. 2004, *MNRAS*, 355, 273
 Czerny, B., Rózańska, A., & Kuraszekiewicz, J. 2004, *A&A*, 428, 39
 Done, C., Madejski, G., & Smith, D. 1996, *ApJ*, 463, L63
 Done, C., Madejski, G. M., Życki, P. T., & Greenhill, L. J. 2003, *ApJ*, 588, 763
 Elvis, M., Risaliti, G., Nicastro, F., Miller, J. M., Fiore, F., & Puccetti, S. 2004, *ApJ*, 615, L25
 Fruscione, A., Greenhill, L. J., Filippenko, A. V., Moran, J. M., Herrnstein, J. R., & Galle, E. 2005, *ApJ*, 624, 103
 Fukazawa, Y., Iyomoto, N., Kubota, A., Matsumoto, Y., & Makishima, K. 2001, *A&A*, 374, 73
 George, I. M., & Fabian, A. C. 1991, *MNRAS*, 249, 352
 Ghez, A. M., Salim, S., Hornstein, S. D., Tanner, A., Lu, J. R., Morris, M., Becklin, E. E., & Duchêne, G. 2005, *ApJ*, 620, 744
 Ghisellini, G., Haardt, F., & Matt, G. 1994, *MNRAS*, 267, 743
 Greenhill, L. J., & Gwinn, C. 1997, *Ap&SS*, 248, 261
 Greenhill, L. J., Jiang, D. R., Moran, J. M., Reid, M. J., Lo, K. Y., & Claussen, M. J. 1995, *ApJ*, 440, 619
 Greenhill, L. J., Moran, J. M., & Herrnstein, J. R. 1997, *ApJ*, 481, L23
 Greenhill, L. J., et al. 2003, *ApJ*, 590, 162
 Guainazzi, M., Fabian, A. C., Iwasawa, K., Matt, G., & Fiore, F. 2005, *MNRAS*, 356, 295
 Hagiwara, Y., Diamond, P., Miyoshi, M., Rovilos, E., & Baan, W. 2003, *MNRAS*, 344, L53
 Hagiwara, Y., Henkel, C., Menten, K., & Nakai, N. 2001, *ApJ*, 560, L37
 Henkel, C., Braatz, J. A., Tarchi, A., Peck, A. B., Nagar, N. M., Greenhill, L. J., Wang, M., & Hagiwara, Y. 2005, *Ap&SS*, 295, 107
 Herrnstein, J. R., Moran, J. M., Greenhill, L. J., & Trotter, A. S. 2005, *ApJ*, 629, 719
 Illarionov, A., Kallman, T., McCray, R., & Ross, R. 1979, *ApJ*, 228, 279
 Ishihara, Y., Nakai, N., Iyomoto, N., Makishima, K., Diamond, P., & Hall, P. 2001, *PASJ*, 53, 215
 Iwasawa, K., Maloney, P. R., & Fabian, A. C. 2002, *MNRAS*, 336, L71
 Iyomoto, N., Fukazawa, Y., Nakai, N., & Ishihara, Y. 2001, *ApJ*, 561, L69
 Kondratko, P. T., Greenhill, L. J., & Moran, J. M. 2005, *ApJ*, 618, 618
 Kondratko, P. T., et al. 2006a, *ApJ*, 638, in press
 Krolik, J., Madau, P., & Życki, P. 1994, *ApJ*, 420, L57
 Kumar, P. 1999, *ApJ*, 519, 599
 Lasota, J.-P., Abramowicz, M., Chen, X., Krolik, J., Narayan, R., & Yi, I. 1996, *ApJ*, 462, 142
 Levenson, N. A., Krolik, J. H., Życki, P. T., Heckman, T. M., Weaver, K. A., Awaki, H., & Terashima, Y. 2002, *ApJ*, 573, L81
 Lodato, G., & Bertin, G. 2003, *A&A*, 398, 517
 Madejski, G., Życki, P., Done, C., Valinia, A., Blanco, P., Rothschild, R., & Turek, B. 2000, *ApJ*, 535, L87

- Magdziarz, P., & Zdziarski, A. 1995, *MNRAS*, 273, 837
- Matt, G. 2002, *MNRAS*, 337, 147
- Matt, G., Bianchi, S., Guainazzi, M., & Molendi, S. 2004, *A&A*, 414, 155
- Matt, G., Brandt, W. N., & Fabian, A. C. 1996, *MNRAS*, 280, 823
- Matt, G., Fabian, A. C., & Reynolds, C. S. 1997a, *MNRAS*, 289, 175
- Matt, G., et al. 1997b, *A&A*, 325, L13
- . 1999, *A&A*, 341, L39
- McHardy, I. M., Green, A. R., Done, C., Puchnarewicz, E. M., Mason, K. O., Branduardi-Raymont, G., & Jones, M. H. 1995, *MNRAS*, 273, 549
- Miyoshi, M., Moran, J., Herrnstein, J., Greenhill, L., Nakai, N., Diamond, P., & Inoue, M. 1995, *Nature*, 373, 127
- Molendi, S., Bianchi, S., & Matt, G. 2003, *MNRAS*, 343, L1
- Neufeld, D., Maloney, P., & Conger, S. 1994, *ApJ*, 436, L127
- Ogle, P. M., Brookings, T., Canizares, C. R., Lee, J. C., & Marshall, H. L. 2003, *A&A*, 402, 849
- Pietsch, W., et al. 2001, *A&A*, 365, L174
- Reynolds, C. S., Fabian, A. C., Makishima, K., Fukazawa, Y., & Tamura, T. 1994, *MNRAS*, 268, L55
- Risaliti, G., Maiolino, R., & Salvati, M. 1999, *ApJ*, 522, 157
- Sako, M., Kahn, S., Paerels, F., & Liedhal, D. 2000, *ApJ*, 543, L115
- Schödel, R., Ott, T., Genzel, R., Eckart, A., Mouawad, N., & Alexander, T. 2003, *ApJ*, 596, 1015
- Schurch, N. J., Roberts, T. P., & Warwick, R. S. 2002, *MNRAS*, 335, 241
- Strickland, D. K., & Stevens, I. 2000, *MNRAS*, 314, 511
- Życki, P. T., & Czerny, B. 1994, *MNRAS*, 266, 653